Symmetry-adapted direct product discrete variable representation for the coupled angular momentum operator: Application to the vibrations of $(CO_2)_2$

Hee-Seung Lee,[a] Hua Chen, and John C. Light
Department of Chemistry and James Franck Institute University of Chicago, Chicago, Illinois 60637

(Received 29 April 2003; accepted 27 May 2003)

The theoretical (quantum) description of large amplitude vibrations of systems containing four or more atoms using orthogonal internal coordinates requires three or more angular coordinates. The basis commonly used to represent these coordinates is the coupled angular momentum basis. We show that a direct product angular discrete variable representation (DVR) can be used advantageously, particularly for systems with high permutation-inversion symmetry and nonlinear equilibrium geometry. The DVR permits full symmetry projection and solution by the sequential diagonalization and truncation method. Application to the dimer of rigid CO_2 demonstrates the accuracy and efficiency of the approach. © *2003 American Institute of Physics.*
[DOI: 10.1063/1.1592511]

I. INTRODUCTION

Over the past ten years, there has been great progress in the field of variational calculations of molecular rovibrational energy levels. Theoretical chemists can now handle the vibrational problems of four-atom systems exactly in full dimension[1–14] and even a five-atom system, such as methane,[15,16] has been tackled. All the bound vibrational levels of some triatomic molecules such as H_3^+[17] and H_2O[18] have been determined very accurately. The progress is in part due to the growing computer power, but more importantly the development of computational algorithms for simplified kinetic energy operators and Hamiltonian evaluation, more efficient basis functions and methods of solution including both iterative and basis reduction methods.

For tetra-atomic systems with orthogonal internal coordinates, a coupled angular momentum (CAM) basis (spherical harmonics),[4,6,10,12–14,19] which is a nondirect product basis, is normally used for the angular part of the basis. The CAM angular basis can be combined with either discrete variable representations (DVR)[20,21] or finite basis representations (FBR)[21] for the radial coordinates. The major advantage of using CAM bases is that the kinetic energy matrix elements are quite simple and all exact matrix elements are finite despite of the singularity in the kinetic energy operator. The CAM basis can be easily adapted to the permutation inversion (PI) symmetries of the system.

To find the eigenpairs with the CAM basis, either an iterative (Lanczos) diagonalization[22] or direct (Householder) diagonalization method can be used. To evaluate the potential matrix by quadrature or the action of the Hamiltonian on a vector in the CAM basis, a pseudo-spectral type transformation to a grid representation[6,10,12,13,23,24] is usually employed in the iterative diagonalization. For accuracy, this transformation is not unitary with more grid points than CAM basis functions. In the direct diagonalization approach, the angular and radial parts are often done using the sequential diagonalization and truncation (SDT) method.[4,25,26] In this procedure the full angular Hamiltonian matrices in CAM basis must be diagonalized, then truncated and coupled with the radial bases to construct the more compact full dimensional Hamiltonian matrix. However, the SDT cannot be applied within the CAM basis itself.

The main problem with the CAM basis is that the number of CAM basis may be very large, even for ''three-angle'' systems. Since the CAM basis functions are delocalized in configuration space, a very large basis may be required if the actual eigenstates are localized in the angles. This is common since the wave functions of the lower energy vibrational states of typical strongly bound tetra-atomic systems are very localized in space. Due to the nondirect product nature of the CAM basis it is not feasible to contract the basis beyond the symmetry reduction.

In theory, direct product representations in each coordinate have several advantages over nondirect product representations such as the CAM basis[2,11,16,27] since an optimal DVR, such as potential optimized DVR[28,29] (PODVR), can be found for each coordinate. This permits both simple Hamiltonian evaluation and efficient matrix vector products in iterative solution methods. The sequential diagonalization and truncation (SDT) techniques can be applied and provides a compact multidimensional correlated basis for direct diagonalization. For these reasons, there has been a growing interest of using direct product DVR for larger polyatomic systems.[2,11,16,27]

However, direct product angular DVR (DPA-DVR) have several potential disadvantages: The size of the direct product basis scales poorly with dimension; symmetries may be difficult to handle; and, perhaps most serious, multidimensional DPA-DVRs cannot be constructed to satisfy the exact wave function boundary conditions at all the singular points of the effective kinetic energy operators (i.e., where the

[a]Electronic mail: seung1@uchicago.edu

$m^2/\sin^2\theta$ type terms become singular). Since the appropriate boundary conditions change depending on the angular momentum projection, no single DVR can be chosen to satisfy all boundary conditions. This leads to ''infinite'' quadrature error for a direct product Legendre polynomial DVR, for example, although the eigenvalues of the kinetic energy operator eventually converge[30] since the effective potentials $(1/\sin^2\theta)$ are repulsive.

The purpose of this paper is to address the issues associated with the above-mentioned problems in the DPA-DVR approach for tetra-atomic systems, namely the symmetry reduction, convergence behavior, and solution by sequential reduction. Specifically, we present an algorithm for the symmetry adaptation of a DPA-DVR which may drastically reduce the number of DVR functions. This allows direct diagonalization for larger systems with high PI symmetry. The number of DVR functions after the symmetrization will be comparable to the number of symmetry-adapted CAM basis functions for a given symmetry block even without the use of a PODVR. If a PODVR basis is appropriate, it could also be symmetrized through the procedure below. The use of symmetry other than parity for the direct product DVRs for the coupled angular momentum operator for three angles (four atoms) has not been reported previously.

The symmetry adaptation of the angular DVR is important since without it the direct product DVR approach may be less efficient than the symmetry-adapted CAM basis even if the SDT procedure is used. Although more DVR functions may be required than the CAM basis for convergence due to the boundary condition problem, the symmetry-adapted direct product DVR approach leads to a much *smaller* three-dimensional angular matrix after the SDT procedure. The symmetry adaptation also has the additional advantage that the assignment of symmetry species to each vibrational state is obviously simplified.

In the present work, we calculated the vibrational energies of the CO_2 dimer, $(CO_2)_2$, using a fully symmetry-adapted direct product DVR basis. With its monomers held rigid, the vibrational Hamiltonian of $(CO_2)_2$ is essentially four dimensional $(J=0)$. But the angular part of the Hamiltonian is identical to that of tetra-atomic system and we can apply the present approach to the tetra-atomic system. There are several motivations to choose $(CO_2)_2$ as a test system: (1) It possesses a very high symmetry (G_{16}) and demonstrates the symmetry adaptation of the angular DVR. (2) It demonstrates that the DPA-DVR is advantageous even for this extremely floppy system for which the CAM functions are reasonably good. Due to the floppiness of the system, a PODVR approach for the angular coordinates may not be appropriate. (3) The floppiness of system will allow the complex to sample the singular region of the Hamiltonian. In this work, we monitor the convergence of the DPA-DVR calculations for such problematic situations. Although the DPA-DVR approach has been used for systems with four or more atoms, the accuracy of the method has not been looked at closely beyond model systems.[30] (4) A variational solution of the $(CO_2)_2$ using the CAM basis is available[31] for checking the accuracy and efficiency of the new approach.

The remainder of the paper is organized in five sections. In Sec. II, we present the theory for the DPA-DVR approach for the vibrational problem of $(CO_2)_2$. The algorithm for the symmetry-adapted DPA-DVR basis is given in Sec. III and the numerical details of the calculation in Sec. IV. We discuss the performance of direct product DVR approach for $(CO_2)_2$ in Sec. V and the conclusion in Sec. VI.

II. THEORY

The direct product angular DVR (DPA-DVR) approach for tetra-atomic systems has been described by several authors.[2,27,32] In this section, we define the method briefly. The coupled angular momentum operator (kinetic energy) for two coupled rotors (rigid linear molecules) is

$$\hat{K}=B_1\hat{j}_1^2+B_2\hat{j}_2^2+B(\hat{J}-\hat{j}_1-\hat{j}_2)^2, \tag{1}$$

where $\hat{j}_i$ is the angular momentum operator of rotor i, B_i is the corresponding rotational constant, J is the total angular momentum, and B is the rotational constant of the whole system. For $J=0$, Eq. (1) represents the angular part of the kinetic energy operator for the vibrational Hamiltonian of tetra-atomic systems. The orientation of the two rotors is given by the two bending angles, with respect to the body-fixed z axis, θ_i, and torsion angle, ϕ.

The operator $\hat{K}$ can be written explicitly as ($\hbar=1$, $J=0$)

$$\hat{K}=(B+B_1)\hat{j}_{10}^2+(B+B_2)\hat{j}_{20}^2+\left(\frac{B+B_1}{1-x_1^2}+\frac{B+B_2}{1-x_2^2}-2B\right)\hat{j}_z^2+B(\hat{j}_{1_+}\hat{j}_{2_+}+\hat{j}_{1_-}\hat{j}_{2_-}), \tag{2}$$

where

$$x_i=\cos\theta_i, \tag{3}$$

$$\hat{j}_{i0}^2=-\frac{\partial}{\partial x_i}(1-x_i^2)\frac{\partial}{\partial x_i}, \tag{4}$$

$$\hat{j}_z=-i\frac{\partial}{\partial\phi}, \tag{5}$$

$$\hat{j}_{1_+}\hat{j}_{2_+}+\hat{j}_{1_-}\hat{j}_{2_-}=\frac{2x_1x_2}{\sqrt{(1-x_1^2)(1-x_2^2)}}\hat{P}_2(\phi)+2\left(\hat{F}(x_1)\frac{x_2}{\sqrt{1-x_2^2}}+\hat{F}(x_2)\frac{x_1}{\sqrt{1-x_1^2}}\right)\hat{P}_1(\phi)+\left(2\hat{F}(x_1)\hat{F}(x_2)-\frac{1}{2}\frac{x_1x_2}{\sqrt{(1-x_1^2)(1-x_2^2)}}\right)\cos\phi. \tag{6}$$

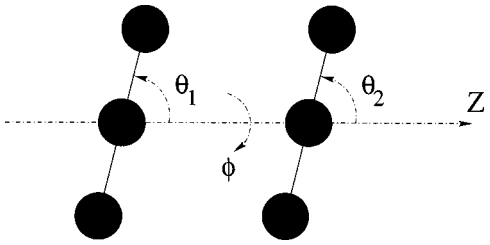

FIG. 1. The Jacobi coordinates for the $(CO_2)_2$.

In the CAM basis all kinetic energy matrix elements are known analytically and only the last operator in Eq. (2) couples different basis functions. In the DPA-DVR, however, the last operator is not analytic and is not numerically Hermitian unless written in the form of Eq. (6). The Hermitian operators, $\hat{P}_i$'s and $\hat{F}$'s in Eq. (6) are defined as

$$\hat{P}_1(\phi) = i \sin\phi \frac{\partial}{\partial\phi} + \frac{i}{2}\cos\phi, \tag{7}$$

$$\hat{P}_2(\phi) = \cos\phi \frac{\partial^2}{\partial\phi^2} - \sin\phi \frac{\partial}{\partial\phi}, \tag{8}$$

$$\hat{F}(x_j) = i\sqrt{1-x_j^2}\frac{\partial}{\partial x_j} - \frac{i}{2}\frac{x_j}{\sqrt{1-x_j^2}}. \tag{9}$$

Note that the Hamiltonian as written in Eqs. (2)–(9) consists of sums of products of Hermitian operators only, which simplifies the use of a DVR.[2]

For the CO_2 dimer, we use Jacobi coordinates, with rigid monomers. The vector $\hat{\mathbf{R}}$ connects the center of masses of the two monomers and lies along the body-fixed z axis (see Fig. 1). The four-dimensional vibrational Hamiltonian can be written as

$$\hat{H} = -\frac{1}{2\mu}\frac{\partial^2}{\partial R^2} + \hat{K} + \hat{V}, \tag{10}$$

where $\hat{V}$ is the potential of the system and R is the length of the vector $\hat{\mathbf{R}}$. In the present work, we used the *ab initio* surface of Bukowski *et al.*[33] for $\hat{V}$.

For the basis functions, we used a potential optimized DVR (PODVR) in the R coordinate. The construction of the PODVR basis for R was described previously.[31] For the angular bases, we used the direct product of Legendre DVRs[21,34] for θ_1 and θ_2, and a Fourier (plane wave) DVR[3,35,36] for the torsion angle ϕ. Thus the DVR is based on the direct product FBR functions

$$\frac{1}{\sqrt{2\pi}}\mathscr{P}_{j_1}(x_1)\mathscr{P}_{j_2}(x_2)e^{im\phi}, \tag{11}$$

where $\mathscr{P}_j$ is a normalized Legendre polynomial. In the Appendix, we describe the details of DVR used in the present work and evaluations of matrix elements in DPA-DVR.

As noted by Dai *et al.*,[30] although the choice of Legendre DVR leads to potentially infinite quadrature errors at the end points ($x=\pm 1$) while evaluating the matrix elements of $\hat{j}_z^2/(1-x^2)$ for $m_z \neq 0$, the eigenvalues of $\hat{j}^2$ do converge to the correct values relatively fast. This is because the effective potential, $1/(1-x^2)$, is repulsive and forces the amplitude of the wave functions to zero in the singular region. However, if the system potential has a strong tendency to make the system sample the singular (linear) region, the convergence becomes slow. This prevents one from using the DPA-DVR approach for linear systems, such as HCCH. In Sec. V, we will come back to this issue and discuss the convergence of the calculations for the vibrational energies of $(CO_2)_2$.

TABLE I. Transformation of angular coordinates and the DVR functions under the actions of PI symmetry operations of G_{16} group.

$\hat{P}$	θ_1	θ_2	ϕ	$\hat{P}\lvert\alpha\beta\gamma\rangle$
E^*	θ_1	θ_2	$-\phi$	$\lvert\alpha\beta\overline{\gamma}\rangle$
(12)(34)	$\pi-\theta_1$	$\pi-\theta_2$	ϕ	$\lvert\overline{\alpha}\beta\gamma\rangle$
(13)(24)	$\pi-\theta_2$	$\pi-\theta_1$	ϕ	$\lvert\beta\overline{\alpha}\gamma\rangle$
(12)	$\pi-\theta_1$	θ_2	$\phi+\pi$	$\lvert\overline{\alpha}\beta\gamma^*\rangle$

III. SYMMETRY-ADAPTED DVR

Symmetry adaptation of basis functions based on permutation-inversion (PI) symmetry have been widely discussed.[37,38] The PI symmetry of the $(CO_2)_2$ can be characterized by using the G_{16} group.[31,37] The group has eight nondegenerate irreducible representations and two doubly degenerate irreducible representations.

As discussed by Carrington[21,39] there are two ways to construct symmetry-adapted DVR bases. The first[40] symmetrizes the original basis functions (FBR basis) and the symmetry-adapted DVR functions are then defined separately for each symmetry block by diagonalizing an appropriate matrix of the coordinate operator. This will not work if the symmetry operations generate a nondirect product basis from the original basis. This occurs for tetra-atomic systems since the symmetry operations involve changes in more than one coordinate. The second approach, which we use here, is more general. We take the linear combinations of primitive DVR functions to generate eigenfunctions of each symmetry operation. Although this is a more natural choice, the structure of the Hamiltonian matrix becomes more complicated.

For the G_{16} group, the actions of the symmetry operations on the body-fixed coordinates have been given [for the $(N_2)_2$ system] by Tennyson *et al.*[41,42] and are shown in Table I. There the numbers refer to the oxygen nuclei and the operation (ab) means the permutation of oxygen nuclei a and b. For details of the PI operations listed in Table I, please refer to Ref. 37. Table I also shows the actions of the PI operations on the DPA-DVR basis, $\lvert\alpha\beta\gamma\rangle = \lvert\alpha\rangle\lvert\beta\rangle\lvert\gamma\rangle$, where $\lvert\alpha\rangle$, $\lvert\beta\rangle$, and $\lvert\gamma\rangle$ represent the DVR functions for θ_1, θ_2, and ϕ localized at DVR points α, β, and γ, respectively. Note that if α, β, and γ are DVR points, $\pi-\alpha(=\overline{\alpha})$, $\pi-\beta(=\overline{\beta})$, $-\gamma(=\overline{\gamma})$ and $\gamma+\pi(=\gamma^*)$ should also be the DVR points to fully adapt the symmetry of $(CO_2)_2$. Our DVR basis functions satisfy these constraints (see Appendix).

The symmetry-adapted DVR basis is obtained by sequentially incorporating the transformation properties of

DVR functions under PI operations listed in Table I. To do this we use the principle that if $\hat{P}$ is a symmetry operation such that $\hat{P}|a\rangle = \pm|b\rangle$, then

$$|a;p=\pm 1\rangle = N_P(|a\rangle + (-1)^p|b\rangle), \tag{12}$$

is the symmetry adapted function with respect to $\hat{P}$. N_P is a normalization constant. This process can be repeated for each symmetry operation sequentially. Since symmetry operations on a DVR function replace coordinate values (see Table I), all unique symmetry-adapted functions can be generated with reduced ranges of the coordinates. The results of the sequential generation of symmetry-adapted DPA-DVR functions for G_{16} are given below, along with normalization constants and the appropriate coordinate range. The symmetry numbers *s*, *l*, *m*, *p*, are 0 or 1 and together generate all symmetrized functions.

A. E^*: The adaptation of inversion operation can be done easily and it is a well known procedure for tetra-atomic systems.[2,3] Namely,

$$|\alpha\beta\gamma;s\rangle = N_s(|\alpha\beta\gamma\rangle + (-1)^s|\alpha\beta\bar{\gamma}\rangle), \tag{13}$$

$$N_s = \sqrt{\frac{1}{2(1+\delta_{\gamma\bar{\gamma}})}},$$

$$\gamma \geqslant 0. \tag{14}$$

Note that the δ-function in the normalization constant also affects the basis function for $\gamma=\pi$ due to the periodic boundary condition (i.e., $\bar{\gamma}=\gamma$ for $\gamma=\pi$). The above-mentioned linear combination leads to DVRs based on $\{\cos m\phi\}$ and $\{\sin m\phi\}$ for the even and odd parity states, respectively.

B. (12)(34): This operation exchanges two oxygen atoms that belong to the same CO_2 monomer. In this case, symmetry-adapted basis function is given as

$$|\alpha\beta\gamma;sl\rangle = N_l(|\alpha\beta\gamma;s\rangle + (-1)^l|\bar{\alpha}\bar{\beta}\gamma;s\rangle), \tag{15}$$

$$N_l = \sqrt{\frac{1}{2(1+\delta_{\alpha\bar{\alpha}}\delta_{\beta\bar{\beta}})}},$$

$$\bar{\alpha} \leqslant \beta \quad \text{if } \alpha \leqslant \alpha_0, \quad \bar{\alpha} < \beta \quad \text{if } \alpha > \alpha_0, \tag{16}$$

where α_0 refers to $\pi/2$ hereafter. In Eq. (16), the range of β is halved. Note that $l=0$ leads to singly degenerate states whereas $l=1$ leads to doubly degenerate states. No further symmetry adaption is possible for the doubly degenerate states. Therefore, the symmetry adaptations described below are applied only for the singly degenerate states.

C. (13)(24): This operation exchanges the roles of two CO_2 monomers and changes the orientation of the body-fixed *z* axis. The symmetry-adapted basis for this operation is given as

$$|\alpha\beta\gamma;slm\rangle = N_m(|\alpha\beta\gamma;sl\rangle + (-1)^m|\beta\alpha\gamma;sl\rangle), \tag{17}$$

$$N_m = \sqrt{\frac{1}{2(1+\delta_{|\alpha||\beta|})}},$$

$$\bar{\alpha} \leqslant \beta \quad \text{if } \alpha \leqslant \alpha_0, \quad \alpha \leqslant \beta \quad \text{if } \alpha > \alpha_0, \tag{18}$$

where $|\alpha| = \max(\alpha,\bar{\alpha})$.

D. (12): This operation affects one of the two monomers and reduce the number of DVR points in ϕ to roughly one quarter of the original number of points. The corresponding symmetry-adapted basis is constructed as

$$|\alpha\beta\gamma;slmp\rangle = N_p(|\alpha\beta\gamma;slm\rangle + (-1)^p|\bar{\alpha}\beta\bar{\gamma}^*;slm\rangle), \tag{19}$$

$$N_p = \sqrt{\frac{1}{2(1+\delta_{\alpha\bar{\alpha}}\delta_{\gamma\bar{\gamma}^*})}},$$

$$0 \leqslant \gamma \leqslant \pi/2 \quad (\alpha \leqslant \alpha_0 \quad \text{if } \gamma = \pi/2). \tag{20}$$

In our implementation of the Fourier DVR for ϕ, only the even numbers of DVR points for ϕ is allowed for $|\alpha\beta\gamma;slmp\rangle$. This is because $|\bar{\alpha}\beta\bar{\gamma}^*;slm\rangle$ does not exist for $\gamma=0$ (i.e., $\bar{\gamma}^*=\pi$) if an odd number of DVR points is used (see Appendix). However, both odd and even numbers of DVR points in ϕ are possible for $|\alpha\beta\gamma;slm\rangle$. In Table II, we summarize the effects of settings for parameters (s,l,m,p). For doubly degenerate states, parameters *m* and *p* are not relevant.

TABLE II. Parameter settings for singly and doubly degenerate states.

Γ	*s*	*l*	*m*	*p*
A_1^+	0/1	0	0	0
A_2^+	0/1	0	1	1
B_1^+	0/1	0	1	0
B_2^+	0/1	0	0	1
E^+	0/1	1		

IV. NUMERICAL DETAILS

The evaluations of Hamiltonian matrix elements in symmetry-adapted angular bases could be quite complicated. We found that the following three-step procedure is easy to implement in the programming. (1) For each symmetry block, we first determine the right combinations of DVR points, (α,β,γ), that satisfy the restrictions on the range of α, β, and γ as described in Sec. III. (2) Expand the symmetry-adapted basis functions, Eq. (19), into 16 primitive basis functions, $|\alpha\beta\gamma\rangle$, and evaluate the matrix elements in the primitive basis. The matrix elements in primitive basis are summed up to obtain the matrix element in symmetry-adapted basis. In other words, we write the matrix elements in symmetry-adapted basis as

$$\begin{aligned}
&\langle \alpha'\beta'\gamma';slmp|\hat{H}|\alpha\beta\gamma;slmp\rangle \\
&\quad = N_s' N_l' N_m' N_p' N_s N_l N_m N_p \{[\langle \alpha'\beta'\gamma'|\hat{H}|\alpha\beta\gamma\rangle + \langle \alpha'\beta'\overline{\gamma'}|\hat{H}|\alpha\beta\overline{\gamma}\rangle + \langle \alpha'\overline{\beta'}\,\gamma'|\hat{H}|\alpha\overline{\beta}\gamma\rangle \cdots] \\
&\qquad + (-1)^s \times [\langle \alpha'\beta'\overline{\gamma'}|\hat{H}|\alpha\beta\gamma\rangle + \langle \alpha'\beta'\gamma'|\hat{H}|\alpha\beta\overline{\gamma}\rangle + \langle \alpha'\overline{\beta'}\,\overline{\gamma'}|\hat{H}|\alpha\overline{\beta}\gamma\rangle \cdots] \\
&\qquad + (-1)^l \times [\langle \overline{\alpha'}\,\overline{\beta'}\,\gamma'|\hat{H}|\alpha\beta\gamma\rangle + \langle \overline{\alpha'}\,\overline{\beta'}\,\overline{\gamma'}|\hat{H}|\alpha\beta\overline{\gamma}\rangle + \langle \alpha'\beta'\gamma'|\hat{H}|\overline{\alpha}\overline{\beta}\gamma\rangle \cdots] \\
&\qquad + \cdots + (-1)^{s+l+m+p} \langle \overline{\beta'}\,\alpha'\,\overline{\gamma'}*|\hat{H}|\alpha\beta\gamma\rangle + \langle \overline{\beta'}\,\alpha'\,\gamma'*|\hat{H}|\alpha\beta\overline{\gamma}\rangle + \langle \beta'\overline{\alpha'}\,\overline{\gamma'}*|\hat{H}|\overline{\alpha}\overline{\beta}\gamma\rangle + \cdots]\}. \qquad (21)
\end{aligned}$$

There are total 256 terms in Eq. (21). However, we have to note that matrix elements in primitive basis with the same form of prefactor (i.e., terms in a given square bracket) are the same due to the symmetry and there are only 16 unique matrix elements in primitive basis. Therefore, this procedure involves 16, instead of 256, evaluations of matrix elements in the primitive basis and it does not consume much CPU time. The evaluations of the matrix elements in the primitive basis are performed as described in Appendix. At this stage, the normalization constants are not considered and some of the terms in the expansion may be identical for certain value of (α,β,γ). (3) Finally, an appropriate normalization factor is multiplied to the result obtained in step 2. The normalization factor will take care of the duplicated terms in step 2.

In the present work, the Hamiltonian matrix was diagonalized using the sequential diagonalization and truncation (SDT) method. First, we diagonalized two-dimensional (2D) Hamiltonian matrix for θ_1 and θ_2 at each DVR point in R and ϕ. We found that including all the terms that are diagonal in R and ϕ, i.e., the first and second terms in Eq. (2), the third term in Eq. (6) and the potential $\hat{V}$ in the 2D matrix leads to the fastest convergence. Once the 2D matrix is diagonalized, a maximum N2D number of states with energies less than E2D are retained. These states coupled with the DVR basis in ϕ are used to construct three-dimensional (3D) angular Hamiltonian matrix at each DVR point in R. In the 3D matrix, the third term in Eq. (2), the first and second terms in Eq. (6) are included. The 3D Hamiltonian matrices are diagonalized and a maximum N3D number of states with energies less than E3D are retained at each DVR point in R. The final 4D matrix is constructed by adding the first term in Eq. (10) and then diagonalized to obtain the vibrational energies and wave functions of $(CO_2)_2$. Note that we can also apply SDT to the θ_1 and θ_2 parts without the loss of accuracy if the 2D matrix diagonalization become time consuming, although this would treat the equivalent θ_1 and θ_2 coordinates differently.

The reduced mass $\mu=21.994\,914\,63$ amu and the monomer rotational constant $B_1=B_2=0.390\,219\,027\ \mathrm{cm}^{-1}$ were used in the calculations. Throughout the calculations, thirteen PODVR points were used for R coordinate that are obtained from 100 Sinc DVR functions distributed in the range of [2.0,7.0] Å. For the angular basis, we used 30 Fourier DVR points in ϕ, but the symmetry adaptation reduces the number of DVR points to 8 for $s=0$ and 7 for $s=1$ calculations, respectively, for singly degenerate states. In the case of bending coordinates, θ, up to 45 DVR points were used. For the SDT parameters, we found that N2D=50, E2D=500 cm^{-1}, N3D=200, E3D=50 cm^{-1} were appropriate to converge the lowest 10 vibrational states of each symmetry block. The typical size of the 4D Hamiltonian matrix in truncated basis is approximately 2000×2000 for each symmetry.

Finally, we make a brief comment on the case where the total angular momentum $J>0$. For $J\neq 0$, the kinetic energy operator $\hat{K}$ in Eq. (1) will have additional terms of $B[\hat{J}^2 - 2(\hat{J}_x\hat{j}_{12,x}+\hat{J}_y\hat{j}_{12,y}+\hat{J}_z\hat{j}_{12,z})]$, where $\hat{j}_{12}=\hat{j}_1+\hat{j}_2$. Assuming that we use symmetric-top eigenfunctions as basis for the overall rotation, the first and the last term are diagonal in K (projection of $\hat{J}$ on the body-fixed z axis), whereas $\hat{J}_x\hat{j}_{12,x} + \hat{J}_y\hat{j}_{12,y}$ (Coriolis coupling) leads to terms in off-diagonal in K. The evaluations of matrix elements for these extra terms in DPA-DVR basis would be more difficult than in the coupled angular momentum (CAM) basis simply because the CAM basis are eigenfunctions of $\hat{J}_z$, $\hat{j}_{12}^2$, and $\hat{j}_{12,z}$. However, the general procedure for diagonalizing the Hamiltonian matrix would be the same: Diagonalize each K-block separately as described above; keep a certain number of states for each K-block; transform off-diagonal K-blocks according to the retained states; and finally diagonalize the transformed Hamiltonian. Alternatively, the Coriolis coupling terms may be included by perturbation theory.

V. RESULTS AND DISCUSSION

The CO_2 dimer has C_{2h} equilibrium structure (slipped parallel, $\theta_1=\theta_2=59°$, $\phi=0°$, see Fig. 2) and there are four intermolecular vibrational normal modes[31,33]

$$\Gamma_{\mathrm{vib}} = 2A_g + A_u + B_u. \qquad (22)$$

By comparing the character tables of C_{2h} and G_{16}, we can find that each vibrational normal mode can be represented as a direct sum of two singly degenerate states and one doubly degenerate state, i.e.,

$$\begin{aligned}
\Gamma_{A_g} &= A_1^+ \oplus B_2^+ \oplus E^+ \\
\Gamma_{A_u} &= A_1^- \oplus B_2^- \oplus E^-, \\
\Gamma_{B_g} &= A_2^- \oplus B_1^- \oplus E^-, \\
\Gamma_{B_u} &= A_2^+ \oplus B_1^+ \oplus E^+.
\end{aligned} \qquad (23)$$

Physically, this means that there are four nonsuperimposible structures for $(CO_2)_2$ (see Fig. 2). If the barriers between these structures are sufficiently high, all four states that constitute each vibrational normal mode are degenerate. In the case of $(CO_2)_2$, however, these barriers are not high enough

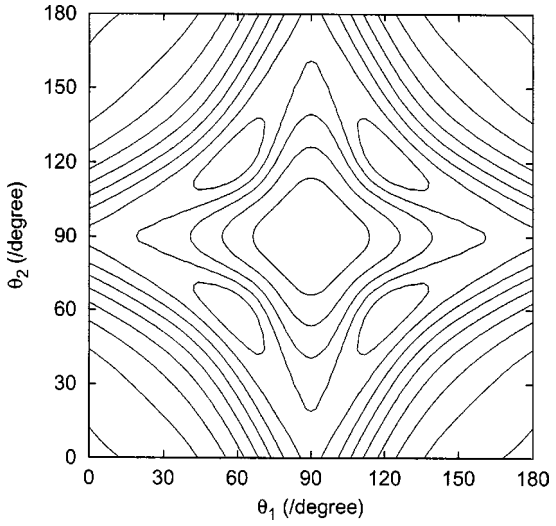

FIG. 2. A two-dimensional contour plot of the $(CO_2)_2$ potential energy surface of Bukowsk *et al.* (Ref. 33) in θ_1 and θ_2. For a given value of (θ_1,θ_2), the potential energy is minimized with respect to R and ϕ. The spacing between lines are 50 cm^{-1} starting at -50 cm^{-1}. The potential has the minimum at -484.0 cm^{-1}.

and moderate vibrational excitation allows the dimer have enough energy to penetrate the barrier. Therefore, each vibrational level is split into four sublevels (tunneling splitting). It should be noted, however, that $(^{12}C^{16}O_2)_2$ is composed of all boson atoms, which means that only the states with A_g symmetry will show up in the real spectrum due to the spin statistics. For different combinations of isotopes, states with other symmetries will also be allowed.

In Table III we report the energies of lowest 10 vibrational states of $(CO_2)_2$ for singly degenerate states calculated by the methods described in the previous sections. For all the DVR calculations reported in Table III, the same DVR and SDT parameters are used (see Sec. IV) except for the number of DVR points in θ. Note that the number of DVR points in θ listed in Table III is referring to the number of primitive basis functions before the symmetry adaptation. It can be seen from Table III that two singly degenerate symmetry blocks listed in the same row have similar energies and they belong to the same vibrational normal mode symmetry [Eq. (23)]. For the ground states, the tunneling splitting is not observed and the ground-state energies are the same (within 0.01 cm^{-1}) for those symmetry pairs, i.e., (A_1^+,B_2^+), (B_1^+,A_2^+), etc.

In Table III, we report the convergence behavior of the lowest 10 vibrational states for each symmetry block with respect to the number of DVR points in θ. We compare the results from the present work with those from the previous work[31] where CAM bases were used. The CAM basis calculations are converged within 0.01 cm^{-1}. In the CAM basis calculations, roughly 900 angular bases were used for each symmetry and the 3D angular Hamiltonian matrices were diagonalized in single step at each PODVR point in R and truncated to construct the 4D Hamiltonian matrix. In the present work, the DPA-DVR with SDT leads to no more than 400 angular bases (truncated 2D basis in θ coupled with Fourier DVR in ϕ). Although a substantially smaller number of angular basis is used in the DPA-DVR approach, we were able to achieve a high accuracy in the calculations. With $N_\theta=45$, the energies of 65 states out of total 80 states reported in Table III differ by less than 0.05 cm^{-1} from those of CAM calculations and 53 of them are within 0.02 cm^{-1}. Given the fact that $(CO_2)_2$ is extremely floppy complex, the number of DVR points needed to achieve the level of accuracy shown in Table III is relatively small, which indicates the good performance of DPA-DVR basis for the coupled angular momentum operator. Note that convergence of calculations with respect to *all* other parameters are achieved within 0.01 cm^{-1} for *all* states listed in Table III. Because CAM basis functions are delocalized in configuration space, they are, in fact, good choices for the van der Waals complexes. This implies that the difference in the size of angular basis between the CAM basis and contracted DVR basis would be greater for more strongly bound systems where the CAM basis becomes less efficient.

Although the overall performance of DPA-DVR basis is excellent, we found there are a few states that converge rather slowly compared to other states. These states are marked with asterisks in Table III. They are the states that are not converged within 0.1 cm^{-1} with $N_\theta=45$, although they are converging to the correct values. These slow-converging states are found only in $A_2^\pm$ and $B_2^\pm$ states, but we could not see any correlation between the convergence and the symmetry. In fact, the symmetry requires different locations of nodal surfaces for $A_2^\pm$ and $B_2^\pm$ states: B_2^+ at $\phi=\pm\pi/2$, A_2^+ at $\phi=\pm\pi/2$, and $\theta_1=\theta_2$, B_2^- at $\phi=0$, A_2^- at $\phi=0$, and $\theta_1=\theta_2$. On the other hand, we can speculate that the nature of these slowly converging states is related to the fact that the DPA-DVR approach is not efficient for the states that sample the singular region. In order to confirm this speculation, we analyzed the wave functions of slow-converging states.

In Fig. 3, we plot the two-dimensional slices of the wave functions in θ_1 and θ_2 coordinates for some of the states marked with asterisks in Table III. They are the tenth B_2^+ state [Fig. 3(a)], eighth A_2^+ state [Fig. 3(b)], ninth B_2^- state [Fig. 3(c)] and third A_2^- state [Fig. 3(d)]. For these plots, the R and ϕ coordinates are fixed at the value where the wave functions are near the maximum. The wave function of tenth A_2^+ state is similar to Fig. 3(b) and wave functions of sixth and ninth A_2^- states are similar to Fig. 3(c). Since the wave function plots in Fig. 3 are reduced dimensional slices of the four-dimensional wave functions, we have to keep in mind that they only provide us part of the information, nevertheless important, about the vibrational motions of the corresponding states even though they represent the wave functions near the maximum amplitude. In fact, we found that small changes in the R coordinate can result in substantially different two-dimensional plots in θ_1 and θ_2, especially for the states with higher excitations.

We first note that the wave functions plotted in Fig. 3 have small amplitude around the global minimum, the slipped parallel structure ($\theta_1=\theta_2=59°$). The eighth A_2^+ state [Fig. 3(b)] and the third A_2^- state [Fig. 3(d)] even have a node at $\theta_1=\theta_2$. The amplitudes of wave functions for the other two states are also pushed away from the global mini-

TABLE III. Convergence of DVR calculations with respect to the number of DVR points in θ for the vibrational states of $(CO_2)_2$. E_{FBR} refers to the energies obtained using CAM basis (Ref. 31). The states that are not converged within 0.1 cm^{-1} with $N_\theta=45$ are marked with asterisks.

		$E_{DVR}-E_{FBR}$						$E_{DVR}-E_{FBR}$			
Symmetry	E_{FBR}	$N_\theta=33$	$N_\theta=37$	$N_\theta=41$	$N_\theta=45$	Symmetry	E_{FBR}	$N_\theta=33$	$N_\theta=37$	$N_\theta=41$	$N_\theta=45$
A_1^+	−392.38	0.00	0.00	0.00	0.00	B_2^+	−392.38	0.00	0.00	0.00	0.00
	−362.93	0.00	0.00	0.00	0.00		−362.93	0.00	0.00	0.00	0.00
	−351.54	−0.01	0.00	0.00	0.00		−351.22	0.00	0.00	0.00	0.00
	−348.03	0.00	0.00	0.00	0.00		−347.92	0.00	0.00	0.00	0.00
	−346.06	−0.03	−0.02	−0.02	−0.01		−343.80	−0.05	−0.04	−0.03	−0.02
	−338.44	−0.03	−0.03	−0.02	−0.02		−332.44	−0.17	−0.13	−0.11	−0.08
	−326.37	−0.02	−0.02	−0.02	−0.02		−323.58	−0.04	−0.03	−0.02	−0.01
	−323.68	0.00	0.00	0.00	0.00		−321.67	−0.09	−0.07	−0.05	−0.04
	−317.96	−0.02	−0.02	−0.02	−0.02		−312.45	−0.08	−0.05	−0.04	−0.03
	−316.69	−0.02	−0.01	−0.01	−0.01		−311.36	−0.30	−0.24	−0.19	−0.15*
B_1^+	−372.69	0.00	0.00	0.00	0.00	A_2^+	−372.69	0.00	0.00	0.00	0.00
	−353.36	−0.01	−0.01	−0.01	−0.01		−353.08	−0.01	−0.01	0.00	0.00
	−345.02	−0.05	−0.04	−0.03	−0.02		−340.76	−0.10	−0.08	−0.06	−0.05
	−334.12	−0.02	−0.02	−0.02	−0.02		−331.25	0.00	0.00	0.00	0.00
	−331.13	0.00	0.00	0.00	0.00		−327.63	−0.17	−0.13	−0.10	−0.08
	−323.55	−0.01	−0.01	−0.01	−0.01		−320.39	−0.15	−0.12	−0.09	−0.08
	−319.41	−0.02	−0.01	−0.01	−0.01		−316.34	−0.03	−0.02	−0.02	−0.01
	−314.87	−0.04	−0.04	−0.04	−0.04		−308.21	−0.26	−0.20	−0.16	−0.12*
	−309.87	−0.02	−0.01	−0.01	−0.01		−302.34	−0.09	−0.06	−0.05	−0.04
	−303.44	−0.04	−0.04	−0.04	−0.03		−300.13	−0.27	−0.21	−0.17	−0.14*
A_1^-	−369.76	0.00	0.00	0.00	0.00	B_2^-	−369.76	0.00	0.00	0.00	0.00
	−342.47	0.00	0.00	0.00	0.00		−342.54	0.00	0.00	0.00	0.00
	−331.37	0.00	0.00	0.00	0.00		−333.37	−0.13	−0.10	−0.08	−0.06
	−327.24	0.00	0.00	0.00	0.00		−328.40	−0.08	−0.06	−0.05	−0.03
	−323.81	0.00	0.00	0.00	0.00		−326.14	−0.05	−0.04	−0.03	−0.02
	−312.22	−0.03	−0.03	−0.03	−0.02		−318.98	−0.18	−0.14	−0.11	−0.08
	−305.47	0.00	0.00	0.00	0.00		−307.17	−0.20	−0.15	−0.11	−0.09
	−300.65	−0.01	−0.01	−0.01	−0.01		−305.26	−0.03	−0.02	−0.02	−0.01
	−293.71	−0.01	−0.01	−0.01	0.00		−299.81	−0.45	−0.34	−0.26	−0.20*
	−289.91	−0.07	−0.07	−0.06	−0.06		−296.51	−0.04	−0.03	−0.03	−0.02
B_1^-	−351.37	0.00	0.00	0.00	0.00	A_2^-	−351.37	0.00	0.00	0.00	0.00
	−334.27	0.00	0.00	0.00	0.00		−335.55	−0.07	−0.06	−0.04	−0.03
	−321.60	−0.02	−0.01	−0.01	−0.01		−327.90	−0.25	−0.19	−0.15	−0.12*
	−312.16	0.00	0.00	0.00	0.00		−314.23	−0.21	−0.16	−0.13	−0.10
	−306.71	−0.02	−0.02	−0.02	−0.02		−312.00	0.00	0.00	0.00	0.00
	−299.79	−0.03	−0.03	−0.02	−0.02		−303.96	−0.40	−0.31	−0.24	−0.18*
	−298.75	−0.01	−0.01	−0.01	−0.01		−302.71	−0.01	0.00	0.00	0.00
	−287.21	−0.05	−0.04	−0.03	−0.03		−293.94	−0.07	−0.05	−0.04	−0.03
	−283.10	−0.03	−0.03	−0.02	−0.02		−291.27	−0.47	−0.36	−0.28	−0.21*
	−280.32	−0.05	−0.05	−0.05	−0.05		−284.24	−0.11	−0.08	−0.06	−0.05

mum structure. The characteristic vibrational motion associated with Figs. 3(a) and 3(b) is the geared in-plane bending motion, which changes the structure of complex from the slipped parallel to the T-shape. Strictly in-plane motion is, however, not allowed in A_2^- and B_2^- states [Figs. 3(c) and 3(d)] since they have node at $\phi=0°$. But, more importantly, all four states plotted in Fig. 3 have non-negligible probability to have the structure close to the T-shape, $\theta_1=0$ and $\theta_2=\pi/2$ (or vice versa), where the singularity occurs. In fact, the tilted T-shaped structure is dominant for the ninth B_2^- state and the third A_2^- state.

These observations confirm that the increasing probability for an eigenstate to sample the singular region (θ_1 or $\theta_2\sim0°$) leads to the slower convergence with respect to the number of DVR points in θ. However, for $(CO_2)_2$ system such problematic states do converge to the correct value without significant deterioration in the accuracy of calculation. As shown in Table III, even the slow-converging states have errors less than 0.1% with $N_\theta=45$. The presence of states sampling the singular region decreases the efficiency of the DVR approach since we have to use more DVR functions, but the impact of such states is drastically reduced by using the symmetry-adapted DVR basis. For typical nonlinear tetra-atomic (or larger) molecules, the probabilities to have linear structures are much lower than what we saw in the $(CO_2)_2$ system unless the molecule is highly excited. Therefore, the convergence problem associated with the singularity in the DPA-DVR approach should be less important for nonlinear tetra-atomic systems and the DPA-DVR basis should be a valuable alternative to the CAM basis up to fairly high internal energy.

Finally, we make a brief comment on the performance of the symmetry-adapted DPA-DVR/SDT compared to the Lanczos based iterative method. One promising way to incorporate the symmetry of the system into the Lanczos method is so called symmetry-adapted Lanczos method of

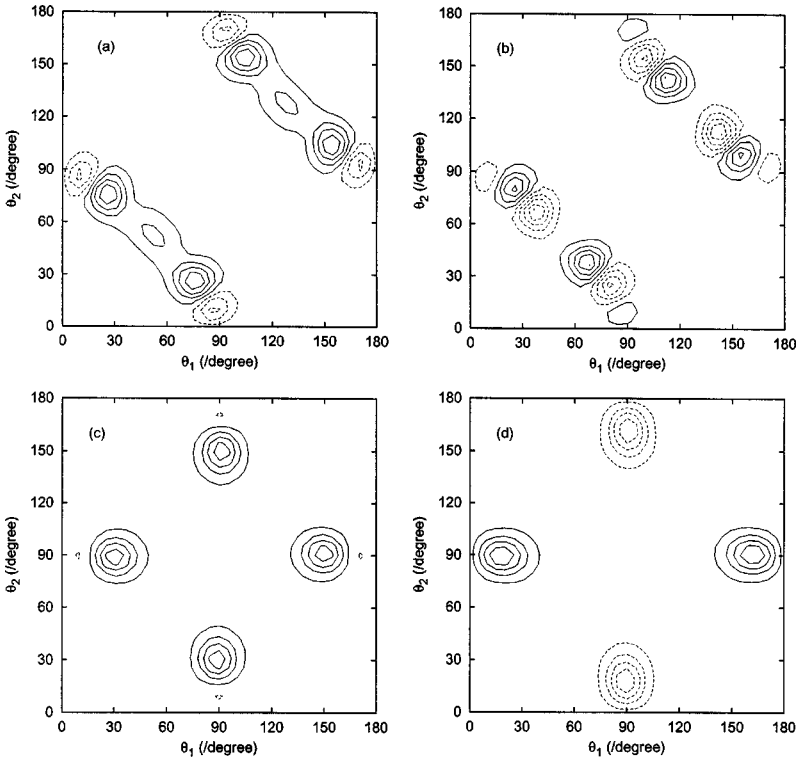

FIG. 3. Two-dimensional slices of the $(CO_2)_2$ vibrational wave function in θ_1 and θ_2 coordinates for (a) the tenth state of B_2^+ symmetry, (b) the eighth state of A_2^+ symmetry, (c) the ninth state of B_2^- symmetry, and (d) the third state of A_2^- symmetry. The other two coordinates, R and ϕ, are fixed at the values where the magnitude of wave function is near the maximum.

Carrington *et al.*[43] and Guo *et al.*[44] In symmetry-adapted Lanczos, Lanczos vectors are symmetrized throughout the Lanczos iteration instead of symmetrizing the basis. If one uses the standard partial summation technique[2,23] for the matrix-vector product, the total operation count for single matrix-vector product is roughly $[10\times N_r(N_\theta)^3N_\phi]$ for the Hamiltonian in Eqs. (2)–(9) with DPA-DVR basis. For the symmetry-adapted DVR/SDT discussed in the present work, the cost of calculation is dominated by the final diagonalization of the 4D matrix, which scales as $(\mathrm{N3D}\cdot N_r)^3$. Since the size of 4D matrix is usually 2000×2000 in this work, the total cost for the direct diagonalization of all symmetry blocks is roughly a factor of 10^2 larger than the cost of a single matrix-vector product with $N_\theta=45$. Since there are other costs that affect the overall performance, it is not trivial to make a direct comparison between the two methods. But the difference in cost between the two methods for calculating lowest 10 states of $(CO_2)_2$ for all symmetry blocks will be small assuming that roughly 10–20 matrix-vector products are needed for each state in symmetry-adapted Lanczos. However, when N_θ (the slowest converging parameter) increases the cost of symmetry-adapted Lanczos is likely to increase more than that of symmetry-adapted DVR/SDT, because the overall cost for the direct diagonalization with SDT is not very sensitive to N_θ,[45] whereas the cost of single matrix-vector product is directly proportional to N_θ^3.

VI. CONCLUSION

The use of direct product angular DVR (DPA-DVR) basis rather than the coupled angular momentum (CAM) bases for systems with more than four atoms has several advantages. The basis can be easily contracted via sequential diagonalization and truncation (SDT) to lead to a much smaller matrix to be diagonalized. It is also trivial to calculate the potential matrix elements in the DVR. The DPA-DVR is particularly useful for a potential that has very localized minima in angles since the CAM basis is delocalized, requiring a large basis. However, the DPA-DVR basis suffers from the poor scaling with respect to the dimensionality and boundary condition problems. This limits the possibility of using the direct diagonalization for tetra-atomic systems, especially for states with large amplitude motions.

In the present work, we present a simple algorithm to construct the fully symmetry-adapted DPA-DVR basis functions for the couple angular momentum operator. An efficient way to evaluate the matrix elements in symmetry-adapted basis is also described. The major advantage of using symmetry-adapted basis is to reduce the required number of DVR basis functions drastically. By symmetrization, the impact of poor scaling is lowered and it is possible to use a DPA-DVR even where a PODVR approach is inappropriate. The present algorithm is applied to the calculations of vibrational energies of $(CO_2)_2$. By using the symmetry-adapted basis and SDT procedure, we were able to achieve high accuracy with considerably (more than a factor of 2) smaller number of angular basis functions compared to the CAM basis. The difference in the size of angular matrix to be diagonalized would be greater for more strongly bound system where the CAM basis becomes less efficient.

We also discuss the issue associated with the improper boundary condition of DPA-DVR approach. As expected, the states that sample the singular regions were found to converge rather slowly compared to other states. But they do converge to the correct values and they are reasonably accurate (errors less than 0.1%) with a moderate number of DVR functions. For a given accuracy, the required number of DVR

functions is larger than what it would be if we do not have such problematic states, but the symmetry adaptation and the SDT method reduce the impact of increasing DVR functions due to those slowly converging states.

ACKNOWLEDGMENT

We are grateful for the support of this research by a grant from the Department of Energy, Grant No. DE-FG02-87ER13679.

APPENDIX: DVR BASIS AND MATRIX ELEMENTS

For Legendre DVR in θ, the DVR points and the FBR-DVR transformation matrix are obtained from the standard procedure.[21,34] Therefore, the DVR points are symmetrically distributed with respect to $\theta=\pi/2$. In the case of Fourier DVR in ϕ, the DVR points are evenly and periodically distributed in $[-\pi,\pi]$, following Meyer's prescription for the definition of DVR points.[35] The DVR points are thus given as

$$\phi_j = j\left(\frac{2\pi}{N}\right), \tag{A1}$$

$$j = \frac{2l-N-1}{2}, \quad \text{(odd N)}, \tag{A2}$$

$$j = \frac{2l-N}{2}, \quad \text{(even N)}, \tag{A3}$$

where N is the number of DVR points and $l=1,2,...,N$. Note that, in Meyer's definition of grid points, $\phi=\pi$ is a grid point for even N, but not for odd N. In addition, $\phi=\pm\pi/2$ are grid points only if N is the integer multiple of 4 and $\overline{\gamma}^*=\gamma$ in this case [see Eq. (19)]. The DVR functions are then defined by

$$u_j(\phi) = \sum_{m=1}^{N} T_{mj}\sqrt{\frac{1}{2\pi}}e^{ik_m\phi} = \sum_{m=1}^{N} T_{mj}\varphi_m(\phi), \tag{A4}$$

where k_m are also given by Eqs. (A2) and (A3) with l replaced by m. The unitary transformation matrix $\mathbf{T}$ is defined as

$$T_{mj} = \sqrt{\frac{1}{N}}e^{-ik_m\phi_j}. \tag{A5}$$

For an odd number of DVR points, this procedure is equivalent to that of Muckerman.[36]

The evaluations of matrix elements in the DPA-DVR basis for the first three terms in Eq. (2) are well known.[3,21,46] In the evaluation of matrix elements for the fourth term in Eq. (2), we need the matrix elements for $\hat{P}_1(\phi)$, $\hat{P}_2(\phi)$, and $\hat{F}(x_j)$ operators in the DVR basis. These are obtained by evaluating the matrix elements in the original basis [Eq. (11)] exactly and then transforming into the DVR. The following relation was used for the "momentum" operator $\hat{F}(x)$

$$\hat{F}(x)\mathscr{P}_l = -\frac{i}{2\sqrt{1-x^2}}\left[(l+1)\sqrt{\frac{2l+1}{2l+3}}\mathscr{P}_{l+1} - l\sqrt{\frac{2l+1}{2l-1}}\mathscr{P}_{l-1}\right]. \tag{A6}$$

Therefore, the matrix elements for $\hat{F}(x)$ in the $\mathscr{P}_l$ involve $\langle\mathscr{P}_{l'}|1/\sqrt{1-x^2}|\mathscr{P}_l\rangle$ which can be evaluated very accurately by using Gauss–Chebychev quadrature of first kind. The matrix elements for the operators $\hat{P}_1(\phi)$ and $\hat{P}_2(\phi)$ in the $\varphi_n(\phi)$ basis are given as

$$\langle\varphi_m|\hat{P}_1|\varphi_n\rangle = \frac{i}{4}[(2k_n+1)\delta_{m,n+1} - (2k_n-1)\delta_{m,n-1}], \tag{A7}$$

$$\langle\varphi_m|\hat{P}_2|\varphi_n\rangle = -\frac{1}{2}[k_n(k_n+1)\delta_{m,n+1} + k_n(k_n-1)\delta_{m,n-1}]. \tag{A8}$$

The matrix elements for the multiplicative operators and the potential are diagonal in the DVR. Therefore, the FBR-DVR transformation matrices in θ and ϕ and Eqs. (A6)–(A8) provide all the necessary ingredients to evaluate the matrix elements of the operator $\hat{K}$ in the DPA-DVR basis.

[1] M. J. Bramley and N. C. Handy, J. Chem. Phys. **98**, 1378 (1993).
[2] M. J. Bramley and T. Carrington, Jr., J. Chem. Phys. **99**, 8519 (1993).
[3] J. Antikainen, R. Friesner, and C. Leforestier, J. Chem. Phys. **102**, 1270 (1995).
[4] D. H. Zhang, Q. Wu, J. Z. H. Zhang, M. von Dirke, and Z. Bačić, J. Chem. Phys. **102**, 2315 (1995).
[5] S. Carter, N. C. Handy, and J. Demaison, Mol. Phys. **90**, 729 (1997).
[6] R. B. Lehoucq, S. K. Gray, D.-H. Zhang, and J. C. Light, Comput. Phys. Commun. **109**, 15 (1998).
[7] N. C. Handy, S. Carter, and S. M. Colwell, Mol. Phys. **96**, 477 (1999).
[8] A. Viel and C. Leforestier, J. Chem. Phys. **112**, 1212 (2000).
[9] D. Luckhaus, J. Chem. Phys. **113**, 1329 (2000).
[10] R. Chen, G. Ma, and H. Guo, J. Chem. Phys. **114**, 4763 (2001).
[11] M. Mladenović, Spectrochim. Acta, Part A **58**, 809 (2002).
[12] D. Xu, G. Li, D. Xie, and H. Guo, Chem. Phys. Lett. **365**, 480 (2002).
[13] H.-G. Yu and J. T. Muckerman, J. Mol. Spectrosc. **214**, 11 (2002).
[14] X.-G. Wang and T. Carrington, Jr., J. Chem. Phys. **117**, 6923 (2002).
[15] D. W. Schwenke and H. Partridge, Spectrochim. Acta, Part A **57**, 887 (2001).
[16] H.-G. Yu, J. Chem. Phys. **117**, 2030 (2002).
[17] M. A. Kostin, O. L. Polyansky, J. Tennyson, and H. Y. Mussa, J. Chem. Phys. **118**, 3538 (2003).
[18] H. Y. Mussa and J. Tennyson, J. Chem. Phys. **109**, 10885 (1998).
[19] M. Mladenović, J. Chem. Phys. **112**, 1070 (2000).
[20] D. O. Harris, G. G. Engerholm, and W. D. Gwinn, J. Chem. Phys. **43**, 1515 (1965).
[21] J. C. Light and T. Carrington, Jr., Adv. Chem. Phys. **114**, 263 (2000).
[22] J. Cullum and R. A. Willoughby, *Lanczos Algorithm for Large Symmetric Eigenvalue Computation* (Birkhäuser, Boston, 1985).
[23] G. C. Corey, J. W. Tromp, and D. Lemoine, in *Numerical Grid Methods and Their Applications to Schrödinger's Equation*, edited by C. Cerjan (Kluwer, Dordrecht, 1992).
[24] G. C. Corey and D. Lemoine, J. Chem. Phys. **97**, 4115 (1992).
[25] Z. Bačić and J. C. Light, Annu. Rev. Phys. Chem. **40**, 469 (1989).
[26] S. E. Choi and J. C. Light, J. Chem. Phys. **97**, 7031 (1992).
[27] H. Chen, Ph.D thesis, University of Chicago (2000).
[28] J. Echave and D. C. Clary, Chem. Phys. Lett. **190**, 225 (1992).
[29] H. Wei and T. Carrington, Jr., J. Chem. Phys. **97**, 3029 (1992).
[30] J. Dai and J. C. Light, J. Chem. Phys. **107**, 8432 (1997).
[31] H. Chen and J. C. Light, J. Chem. Phys. **112**, 5070 (2000).
[32] M. Mladenović, Spectrochim. Acta, Part A **58**, 795 (2002).
[33] R. Bukowski, J. Sadlej, B. Jeziorski, P. Jankowski, K. Szalewicz, S. A. Kucharaski, H. L. Williams, and B. M. Rice, J. Chem. Phys. **110**, 3785 (1999).
[34] J. V. Lill, G. A. Parker, and J. C. Light, Chem. Phys. Lett. **89**, 483 (1982).
[35] R. Meyer, J. Chem. Phys. **52**, 2053 (1970).
[36] J. T. Muckerman, Chem. Phys. Lett. **173**, 200 (1990).
[37] P. R. Bunker and P. Jensen, *Molecular Symmetry and Spectroscopy* (NRC, Ottawa, 1998).

[38] A. van der Avoird, E. H. T. Olthof, and P. E. S. Wormer, J. Chem. Phys. **105**, 8034 (1996).
[39] N. M. Poulin, M. J. Bramley, T. Carrington, Jr., H. G. Kjaergaard, and B. R. Henry, J. Chem. Phys. **104**, 7807 (1996).
[40] R. M. Whitnell and J. C. Light, J. Chem. Phys. **89**, 3674 (1988).
[41] J. Tennyson and A. van der Avoird, J. Chem. Phys. **77**, 5664 (1982).
[42] J. Tennyson and A. van der Avoird, J. Chem. Phys. **80**, 2986 (1984).
[43] X.-G. Wang and T. Carrington, Jr., J. Chem. Phys. **114**, 1473 (2001).
[44] R. Chen and H. Guo, J. Chem. Phys. **114**, 1467 (2001).
[45] Only the cost of lower dimensional diagonalizations increase since the size of final 4D matrix does not depend on N_θ.
[46] S. E. Choi and J. C. Light, J. Chem. Phys. **92**, 2129 (1990).